Adhesive wear of a Ti6Al4V tribopair for a fast friction contact

G. Chassaing [a,d], L. Faure [b], S. Philippon [a,*], M. Coulibaly [a], A. Tidu [c], P. Chevrier [a], J. Meriaux [d]

a Laboratoire de mécanique Biomécanique, Polymère, Structures, EA4632, Ecole Nationale d'Ingénieurs de Metz (ENIM), 1 route d'Ars Laquenexy, Metz, France
b Laboratoire d'Étude des Microstructures et de Mécanique des Matériaux (LEM3), CNRS UMR 7239, Université de Lorraine, Metz, France
c Laboratoire d'Étude des Microstructures et de Mécanique des Matériaux, CNRS UMR 7239, Ecole Nationale d'Ingénieurs de Metz, 1 route d'Ars Laquenexy, Metz, France
d SNECMA, groupe SAFRAN, Moissy-Cramayel, France

Friction tests at high sliding velocity are carried out by subjecting specimens to an apparent normal pressure of 110 MPa in the range of 40–64 m/s to reproduce severe conditions of contact between the rotating blades and the rotor in aircraft engines. Therefore, impacts of a projectile against a fixed sample are carried out for the investigation of a pair of Ti6Al4V materials. A mean coefficient of friction has been ascertained by two types of method: a tribometer device and an energetic approach. A slight sensitivity of the coefficient of friction with respect to the sliding velocity is observed. Postmortem analyses of samples reveal a decomposition of the frictional subsurface in multiple distinct layers: initial micro-structure, severe plastic deformation (shear strain up to 16), phase transformation ($T > 980\ ^{\circ}C$) and material transfer. A scenario of the adhesive wear mechanism is proposed in four steps.

1. Introduction

The future efficiency of aircraft engines is related to the design of parts able to support the increase of applied forces considering a limited mass. For this purpose, materials must offer a high strength/weight ratio. Aluminium alloys can meet this requirement as long as the temperature is low ($T < 130\ ^{\circ}C$) while the properties of titanium alloys allow operating in severe environment conditions where temperature is close to a few hundreds of degrees Celsius [1]. The components of a low pressure compressor made of titanium alloys are designed to work at temperatures up to 600 °C. The mechanical bond between the rotating blades and the slot of the rotor is usually subjected to fretting fatigue solicitation under high pressure. Even if some research investigations have provided results showing an improvement in the reliability and the design of these parts, there is little information in exceptional cases such as bird ingestion or compressor blade off. Under these extreme conditions, the interface of contact can suddenly slide by a few millimeters at high velocity ($30\ m/s > V > 40\ m/s$) for an apparent normal pressure p ranging between 300 MPa and 400 MPa.

The energy dissipated during this friction process produces high local temperatures at the contact up to 1000 °C or more [2]. Unfortunately the microstructure of Ti6Al4V is strongly dependent on the temperature. The Ti6Al4V alloy is allotropic with a HCP lattice, α phase, up to 980 °C and a BBC lattice, β phase, above this temperature value. The tribological properties of titanium alloys are still not very well known in the conditions presented previously. Understanding this phenomenon interaction under high pressure and high sliding velocity could significantly improve mechanical reliability of contact interfaces, and consequently the lifespan of the components.

The friction process is generally characterized by the coefficient of friction (COF) μ defined by the Amontons/Coulomb law. As indicated in Eq. (1), it is obtained by calculating the ratio between the force opposite to the movement, noted F_T, and the normal force applied at the sliding interface F_N.

$$\mu = \frac{F_T}{F_N} \tag{1}$$

Concerning the steel-on-steel dry friction, Lim et al. [3] gather many results from various studies according to which two distinct tribological behaviors are observed. For velocities up to 1 m/s, the friction coefficient μ mainly depends on the roughness of the samples. For higher values of V, μ depends on the sliding velocity and/or the normal pressure. Among few studies on the tribological behavior of titanium alloys, Qiu et al. [4] use a pin on disk tribometer to study friction between a Ti6Al4V pin and a steel GCr15 counterface over a slip distance up to 7000 m. The range of velocities spreads from 30 to 70 m/s for a normal pressure varying

* Corresponding author. Tel.: +33 387346668.
E-mail address: philippon@enim.fr (S. Philippon).

from 0.33 MPa to 1.33 MPa. This kind of experiment is usually dedicated to the investigation of wear, wear rate and damage induced.

The results highlight the friction coefficient decrease with the increase of the sliding velocity and the apparent normal pressure. Severe plastic deformation and melting damage are observed on the worn surface of Ti6Al4V. The main wear mechanism is identified as an adhesive wear. Authors observe as well that the wear rate increases with the product pV. In a recent work [5], a Ti6Al4V-on-Ti6Al4V contact is considered under a normal pressure close to 40 MPa. For a sliding velocity ranging from 0.1 to 3.7 m/s, the coefficient of friction increases with velocity. The mechanical work combined with the low thermal conductivity of the titanium leads to a high temperature at the interface. A multilayer decomposition is observed: phase transformation, plastically strained layers, and material transfer. Microstructural analysis points out phase changes such as $\alpha \rightarrow \beta$ above transus β ($T > 980$ °C) and subsequently a rapid quench leading to α' martensite creation.

These experimental parameters are in fact quite remote from the extreme conditions previously detailed. The aim of this work is thus to investigate the effects of the sliding velocity ranging from 40 to 64 m/s under an apparent normal pressure close to 110 MPa on a Ti6Al4V tribopair. After focusing on existing experimental methods enabling to reach quasi-instantaneously sliding conditions under high pressure, the present experimental device and tests are described in the second section. Friction tests are performed in order to determine the evolution of COF and to measure the associated wear. The induced changes on microstructure of worn materials are reported in the third section of this paper. Finally, the damage mechanisms observed on the friction path complete this study.

2. Measurement of the dry friction coefficient

Scientific literature provides many devices dedicated to friction investigation. Their capacities are very different in terms of normal pressure, sliding velocity and also process duration. Only a few of them meet requirements such as quasi-instantaneous loading and sliding velocity varying from a few centimeters per second to a few tens of meters per second. So, the standard solution consisting of a pin tip sliding against a rotating disk cannot be considered here. In addition, the inevitable running-in period before reaching stationary sliding conditions clearly changes the initial surface by successive overlappings.

To obtain the frictional conditions described further above, the plate impact experiments or the modified Kolsky bar apparatus are usually well adapted. The first solution is designed to investigate the transient frictional response of contact interfaces sliding from 1 to about 18 m/s with a normal pressure up to 3 GPa and more [6]. Although these parameters satisfy the requirements of this study, the technique is still complex, and above all, the sliding length does not exceed 250 μm. Concerning the second solution, the device is modified to combine an elastic torsional wave with a static compressive force in order to control the interfacial loading. For that purpose, an input tube impacts a rotating output one [7,8]. This technique and its variants [9,10] aim to investigate the dry sliding for pressures and velocities varying up to 100 MPa and 20 m/s respectively. In this case, the friction length is greater than the one obtained from plate impact experiments (i.e. 10 mm).

The setup used in this work allows the study in a large range of velocities (from 0.1 to 100 m/s) under an apparent normal pressure around one hundred of megapascals but also for a sliding length of 60 mm. The tribometer device was initially designed and developed by Philippon et al. [11,12]. A significant enhancement was conducted in order to also measure the normal force applied during the interaction process [13,14,5]. In this paper, the apparatus is adapted on a ballistic bench to reach higher velocities. Fig. 1 gives an overview of the test bench and the layout of the different parts of the equipment. A short description of the tribometer device is proposed here in order to explain the role played by the two components in the measurement of the forces, see Fig. 2. The first one is a dynamometer ring that applies a known normal force F_N on the interface of samples. Its intensity is calibrated by the

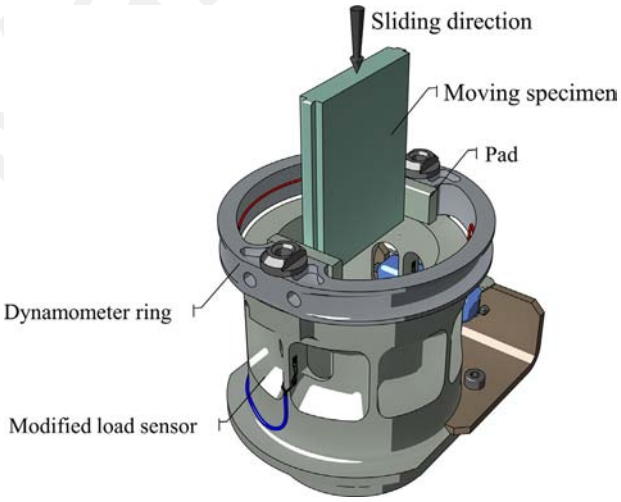

Fig. 2. Version of the updated tribometer device.

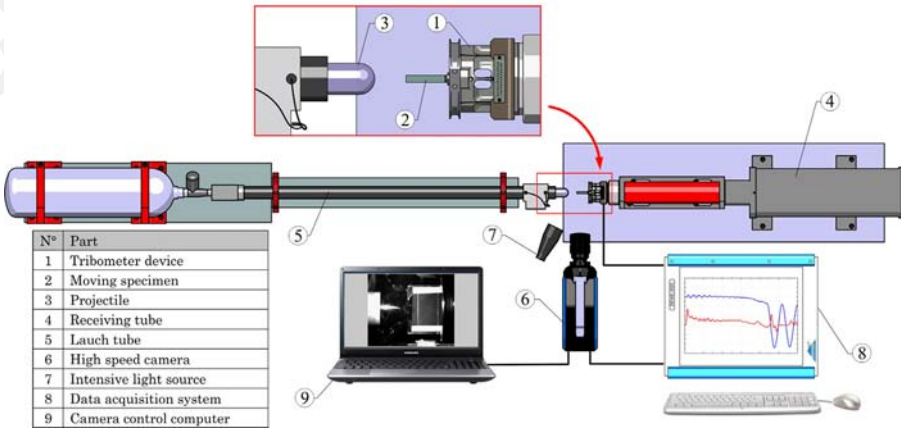

N°	Part
1	Tribometer device
2	Moving specimen
3	Projectile
4	Receiving tube
5	Lauch tube
6	High speed camera
7	Intensive light source
8	Data acquisition system
9	Camera control computer

Fig. 1. Overview of the friction apparatus adapted on a ballistic bench.

elastic deformation of the ring. This deformation is due to the dimensions of the two fixed pads and the specimen. A set of two strain gauges, connected to form a Wheatstone half-bridge, is glued onto the inner side of the ring. The frictional force F_T induced by the relative movement of the specimen against the pads produces an elastic deformation on the second part (load sensor). Similarly two sets of strain gauges are attached to this component. The normal and frictional forces are monitored and recorded all along the friction process.

The energy required for the specimen motion results from the impact of a massive projectile that excites the whole structure and consequently interferes with the measurements. Therefore, the stiffness of the last version of the tribometer device has been increased in order to improve the dynamic behavior of the sensor during the fast loadings. This new sensor is 18% stiffer than the previous version. As previously described [13,14], a calibration is similarly carried out on a tensile machine. Sensitivities of the load sensor and the dynamometer ring are respectively equal to 7.9 N V/mV and 1.7 N V/mV. Thereafter, the results showed that it is unnecessary to correct inertial effects [15]. Accordingly, only a low-pass filter (10 kHz) is used for the post-treatment of the recorded forces and no change in the dynamometer ring design is made.

Note that temperature measurements during interaction would provide interesting information. The use of experimental conventional techniques (thermographic camera, embedded thermocouples) is unfortunately restricted by the confinement of the contact. There are some remarks about the application of these techniques to our set-up. In order to place a thermographic camera close to the contact surface, one of the parts have to be drilled. This geometry modification of the plane–plane contact tends to alter the temperature field by introducing edge effects. Concerning the use of embedded thermocouples, different holes through the thickness of the fixed part are needed. As above, the number and location of holes modify the heat diffusion. For instance, when thermocouples are inserted parallel to the sliding direction, the measurement error can reach 50% [16]. So, no measurements are developed here. Moreover, thermal information is provided in the results section by using phase changes on Ti6Al4V microstructure.

3. Forces acquisition and postmortem analysis

3.1. Experimental setup

All the tests are carried out on a ballistic bench, see Fig. 1. Cylindrical projectiles with hemispherical tip are propelled by means of a high pressure gas gun. For this, compressed air or nitrogen is chosen according to the target sliding velocity. The maximum velocity achievable with 0.5 kg projectiles reaches around 90 m/s. The velocity of the projectile is measured at the exit of the launch tube with a set of two laser photodiodes, just before the impact of the specimen. Nevertheless, the imbalance of masses between the projectile and the specimen (combined with a normal load applied on samples) leads to a poorly controlled sliding velocity compared to that of the impact. Consequently, in order to monitor the real or instantaneous velocity during the friction process, a high speed camera Shimadzu HPV2 has been used. This camera allows the capture of 102 single frames with a maximal rate of 1 million frames per second. The resolution is maintained at 312×260 pixels all along the acquisition sequence whatever the recording speed. The trigger of the camera is synchronized by the impact of the projectile on the back of the moving specimen. Intensive light sources combined with optical fibers provide the necessary light intensity for the video capture.

During the test, the raw signals from the two parts of the tribometer device – namely the dynamometer ring (providing and measuring the normal force) and the load sensor (measuring the tangential force) – are recorded with a sample rate of 400 kHz. The sliding specimen and the projectile are caught in the receiving tube allowing the postmortem analysis of the sliding surface of the specimen.

Fig. 3 presents an example of force acquisition for a 40 m/s impact velocity. The recorded signal may be divided into three distinct zones. The first zone corresponds to the beginning of the interaction. The initial impact of the projectile on the back of the test-piece generates an inertia peak on the tangential force signal and simultaneously causes some fluctuation on the normal force. Within this transitional period the process of friction is not balanced and the signals are not to be considered. In the second zone, normal and tangential forces are relatively constant and only slight variations in their amplitudes are observed. Average values of the normal and tangential forces coming from the data acquisition system are exploited to extract the mean coefficient of friction μ. The exit of the moving specimen from the dynamometer ring causes the decrease of the normal force and marks the beginning of the third zone. Indeed, during this period it is noted that the contact surface gradually decreases. The rear surfaces of both specimen and pads are subjected to an extremely high increase of the normal pressure at the end of the interaction.

The sequence of an interaction at $V=40$ m/s and $p=110$ MPa is presented in Fig. 4. Each frame of the recording is analyzed with a software programme allowing the determination of the specimen position at different known times. The dispersion of the dots displayed here is a result of the combination of the short process duration (2 ms), the relatively weak of the CCD sensor resolution (312 pixels in length) and the camera lens. A linear interpolation of these data illustrates the variation of the sliding velocity generated by the frictional work.

The recording ensures that the projectile is no longer in contact with the sample after impact, as shown in Fig. 4. Only frictional forces modify the velocity of the moving specimen. The decrease of the specimen kinetic energy can be used to determine the mean COF during the interaction.

In this case, the variation of kinetic energy ΔE_k between two distinct times t_i and t_j is given as follows:

$$\Delta E_k = \frac{1}{2}\, m(V_j^2 - V_i^2) \tag{2}$$

where

- V_i and V_j are respectively the velocities at times t_i and t_j,
- m is the moving specimen mass.

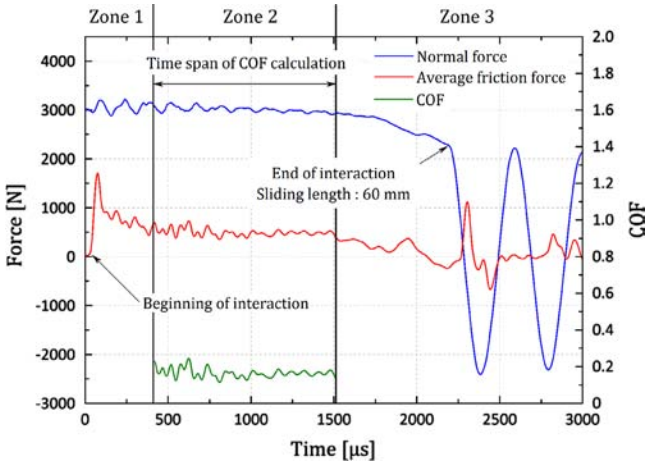

Fig. 3. Typical recording of a friction test – Ref E41_V40.

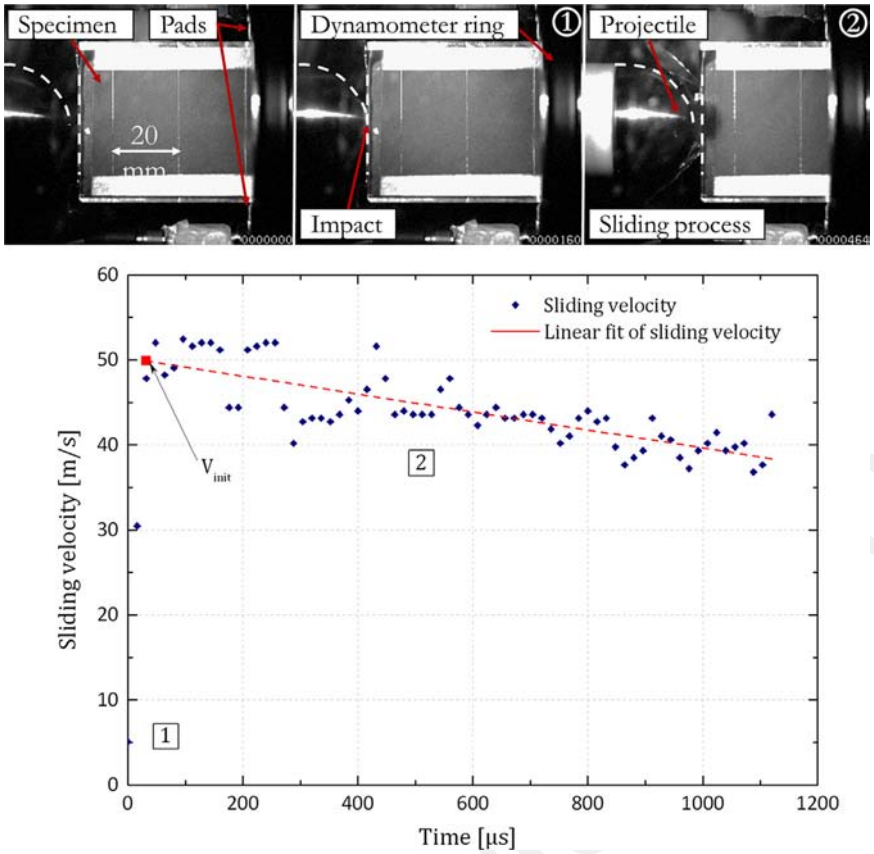

Fig. 4. Instantaneous sliding velocity measurement by ultra high speed camera – Ref E30_V50.

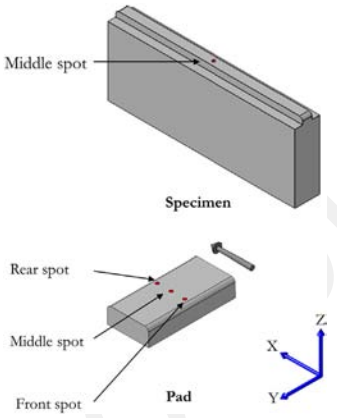

Fig. 5. Location of the observation zones.

Using the Coulomb law and assuming that μ is similar on both stationary pads, the variation of frictional work for a sliding distance L_{i-j} may be expressed as a function of the measured normal force F_N:

$$\Delta W_{i-j} = 2\,\mu\,F_N\,L_{i-j} \tag{3}$$

Equality between the variation of kinetic energy and the work of frictional forces leads to the determination of the average calculated COF μ_E:

$$\mu_E = \frac{m(V_j^2 - V_i^2)}{4\,F_N\,L_{i-j}} \tag{4}$$

This average value μ_E is compared in the next section with measured μ. This way to work out an average coefficient of friction is used later to validate the experimental results.

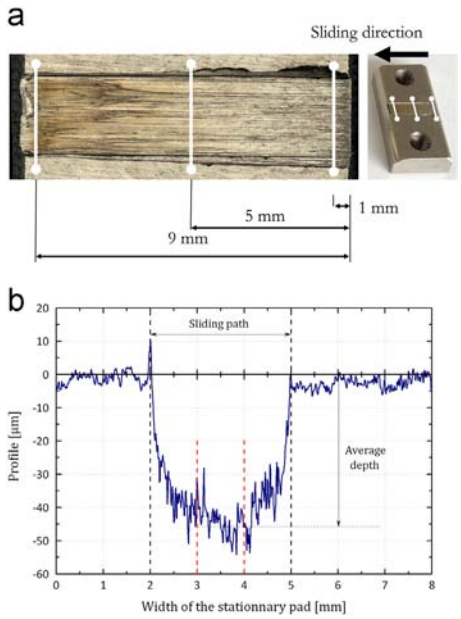

Fig. 6. Profile measurement. (a) Zones of measurement. (b) Example of a measured profile.

3.2. Postmortem analysis

Changes on microstructure induced by different sliding velocities are investigated using a scanning electronic microscope (ZEISS Supra 40). SEM observations are made for cross sections of the sample (*XZ* plane as shown in Fig. 5). The moving specimen

is only examined near its central region while the stationary pad is analyzed at the front, middle and rear of the friction path.

Postmortem profile measurements are performed using an optical 3D microcoordinate system (Alicona Infinite focus). As mentioned before, the stationary pad is studied on three spots (front, middle and rear) as described in Fig. 6(a). In Fig. 6(b), the wear profile depth is clearly defined on a width of 3 mm (corresponding to the width of the sliding path) and its mean value is calculated at the central position. The wear volume is evaluated by a volumetric measurement.

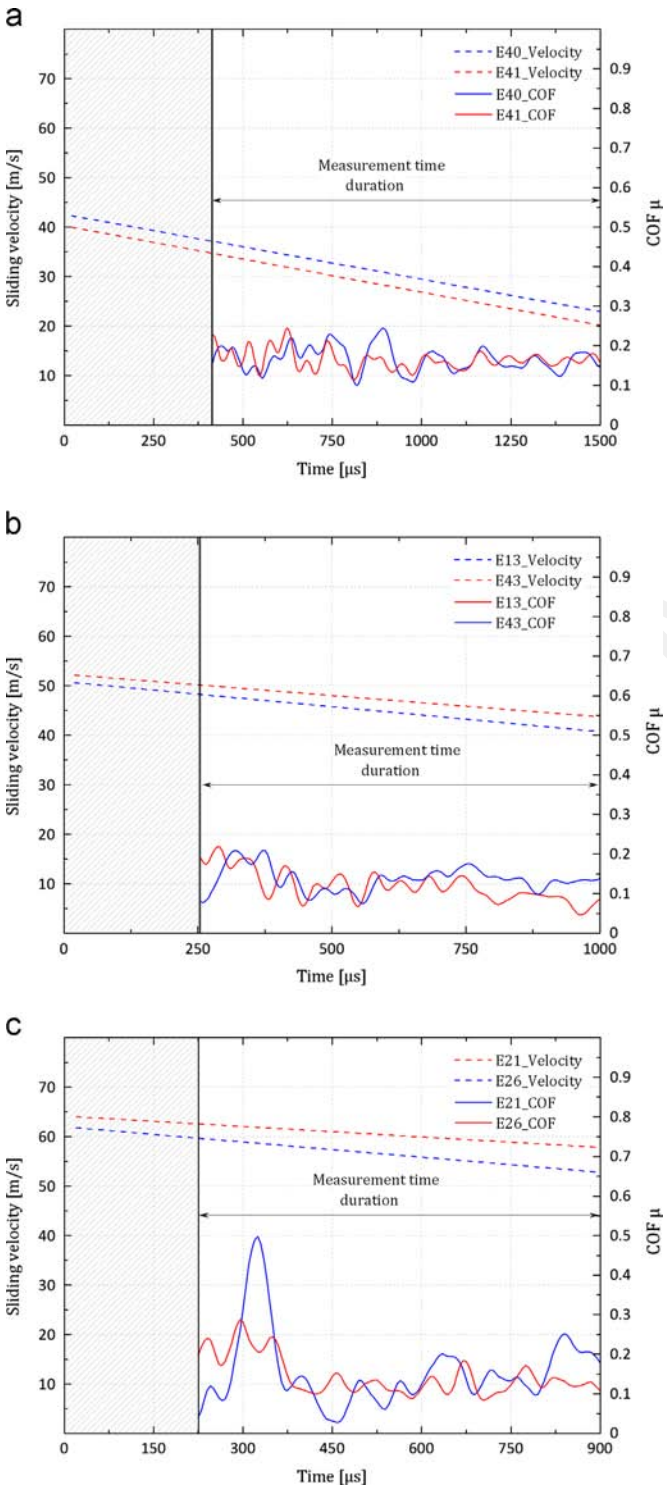

Fig. 7. COF and the sliding velocity evolution for an apparent normal pressure of 110 MPa and for different impact velocities. (a) $V_{impact} = 30$ m/s, (b) $V_{impact} = 40$ m/s, and (c) $V_{impact} = 60$ m/s.

4. Experimental results and discussion

4.1. Measurement of the dry friction coefficient for a Ti6Al4V-on-Ti6Al4V setup

All the tests are taken into account with calculated initial velocities V_{init} ranging from 40 to 64 m/s and an apparent normal pressure kept at 110 MPa. Each configuration is repeated twice. Fig. 7 presents the whole results involving the evolutions of the friction coefficient and the sliding velocity.

The initial and final velocities (V_{init} and V_{fin} respectively) evaluated by means of the acquisition video, as well as those of the projectile, are reported in Table 1. The calculation of the average friction coefficient μ_E is derived from the velocity drop as defined above (Eq. (4)). Despite the discrepancy in plotting dots, both μ_E and μ are quite similar (see Fig. 8).

The outcomes point out the good repeatability of the tribometer device measurements greater. For the range of studied velocities, the mean value of COF decreases very slightly or even remains almost unchanged as the velocity increases.

4.2. Sub-surface characterization

4.2.1. Postmortem analysis of moving specimen

SEM observations of the moving specimen for an initial sliding velocity V_{init} of 40 and 64 m/s are presented in Fig. 9. These pictures reveal that the multi-layer decomposition proposed by Faure et al. [5] is also confirmed for this range of velocities. As

Table 1
Values of impact velocities, real velocities and dry coefficients of friction.

Test reference	Impact velocity (m/s)	Calculated velocity (m/s)		Loss of velocity (%)	Average calculated COF	Average measured COF
	V_{impact}	V_{init}	V_{fin}		μ_E	μ
E40_V40	34	43	13	70	0.22	0.17
E41_V40	33	40	10	75	0.20	0.16
E43_V50	43	52	40	23	0.14	0.14
E13_V50	44	50	35	30	0.16	0.12
E26_V60	65	61	50	18	0.16	0.15
E21_V60	60	64	56	13	0.13	0.15

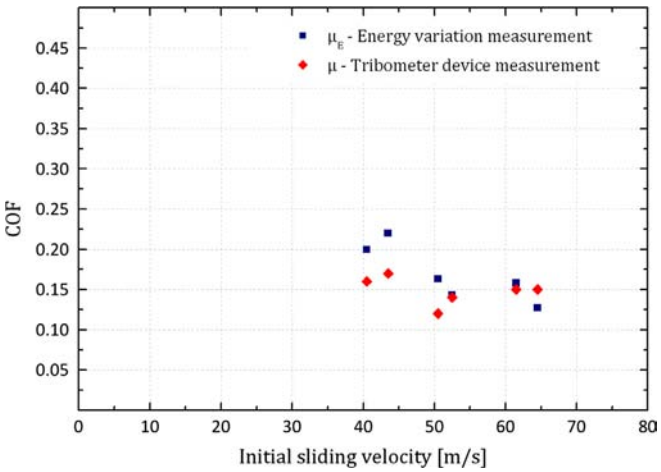

Fig. 8. COF μ and μ_e as a function of the initial sliding velocity V_{init}.

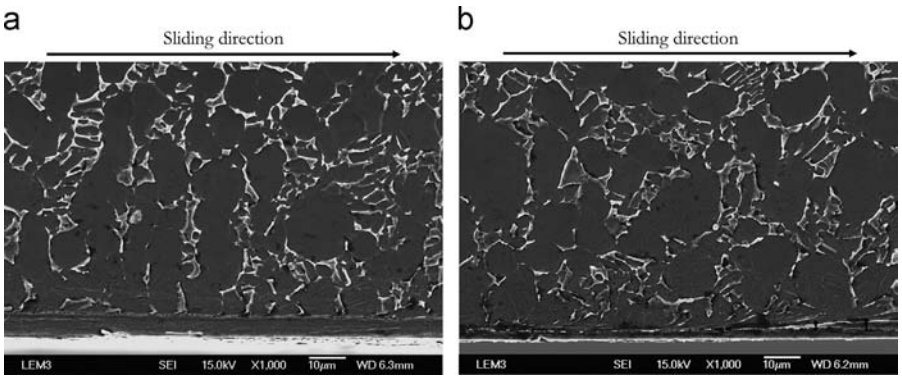

Fig. 9. SEM observations of the moving sample. (a) Initial velocity: 40 m/s, normal pressure: 110 MPa – Ref E41_V40. (b) Initial velocity: 64 m/s, normal pressure: 110 MPa – Ref E21_V60.

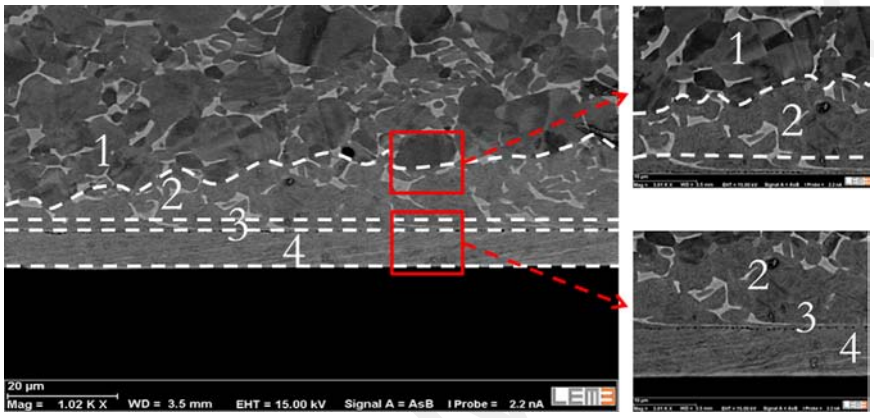

Fig. 10. Sub-layer decomposition of the microstructure of the moving specimen.

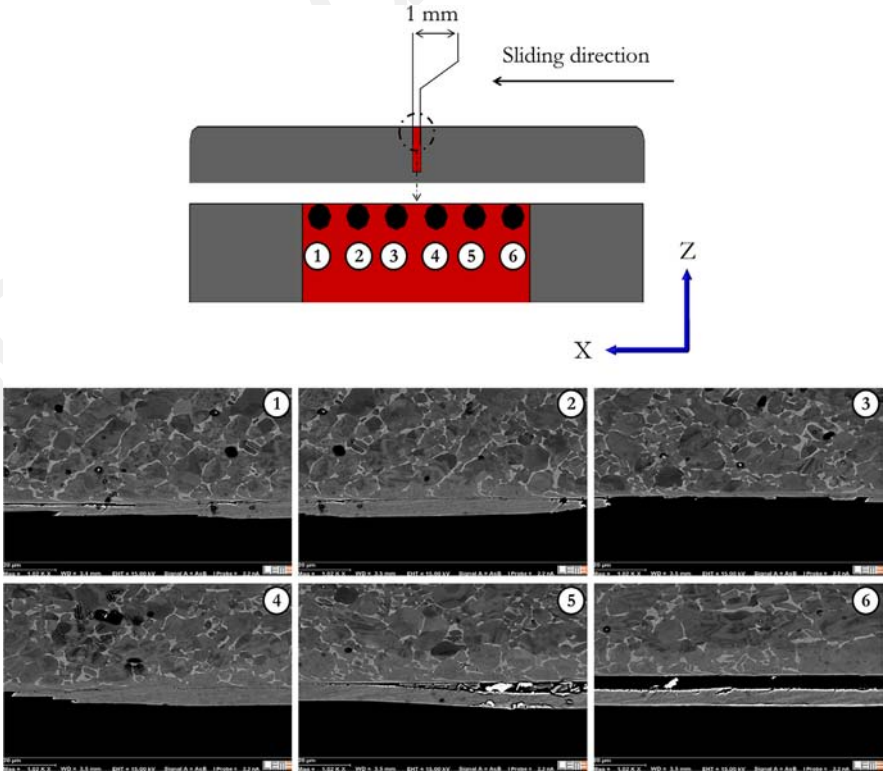

Fig. 11. Postmortem analysis of the transferred layer: SEM observations for 1 mm sliding length.

illustrated in Fig. 10, the transition borders between the sub-layers can be clearly identified (dashed lines).

Zone 1 corresponds to the as-received material consisting of quasi-equiaxe α and inter-granular β grains. Zone 2 is characterized by a thin lamellar microstructure corresponding to the α' martensitic phase. During the experiments, transus β temperature is reached, then after a rapid cooling, a α' martensite microstructure is produced although initial β grains are still visible. From Puerta Vellasquez et al.'s work [17], a similar behavior is observed for a fast cooling of 50 000 °C/s (value estimated by numerical simulation).

Within zone 3, β grains are dragged along the sliding direction through a few micrometers thickness. Zones 2 and 3 in which the temperature is higher than 980 °C corresponds to the thermal affected zone (TAZ).

For both sliding velocities of 40 and 64 m/s, the thickness of the TAZ remains similar (around 20 µm). Consequently, the increase of the mechanical frictional energy calculated from the product $\mu F_N V$ has no effect on each sub-layer thickness.

The material transfer from the pad defines to zone 4 and is a typical event of adhesive wear. Faure et al. [5] attributes it to thermal softening. This occurrence was already observed and described by Fernandes et al. [18] for a steel-on-steel contact.

In there paper, they took under consideration the dependence of the formation of a friction film on mild and severe wear effects. Thus, characteristics of this film can be determined by the examination of milled and compacted wear debris. In the case of mild wear, a thick and homogeneous layer is observed, while for severe wear, a thin and non-continuous film is noticed. The thickness and the uniformity of the layer decrease with the severity of the test condition. As shown in Fig. 11, a non-continuous layer is observed for six positions along 1-millimeter sliding length.

4.2.2. *Postmortem analysis of fixed pad*

SEM observations and microgeometrical profile measurements of the stationary pad for initial sliding velocities V_{init} of 40 and 64 m/s are displayed in Fig. 12. As for the moving specimen, the thickness of the plastically deformed region (zone 3) is similar for both sliding velocities. The sub-layer decomposition previously defined remains valid despite the no transferred material layer. In this part, this layer is no longer observable and a wear process appears along the sliding track.

In order to evaluate the evolution of this wear and the TAZ thickness (zones 2 and 3), postmortem analysis of the stationary

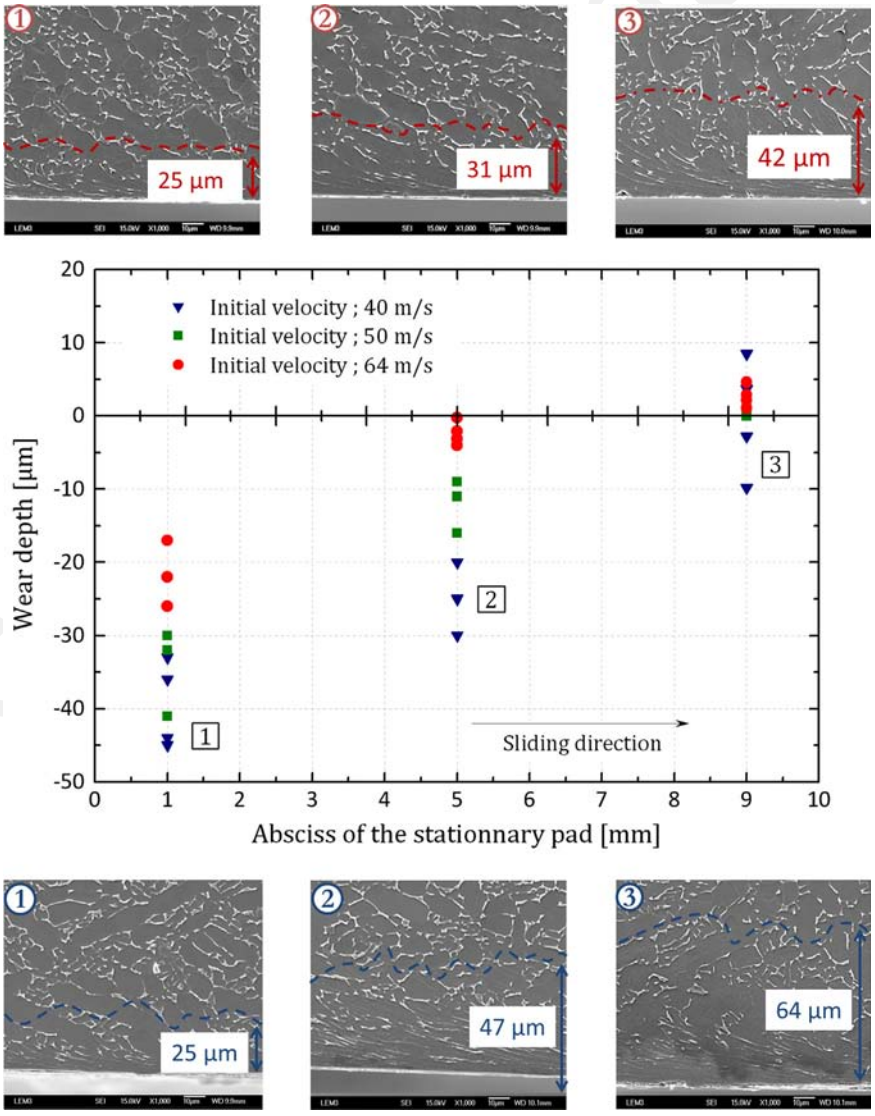

Fig. 12. Profile measurements and SEM observations of the pad for all tests.

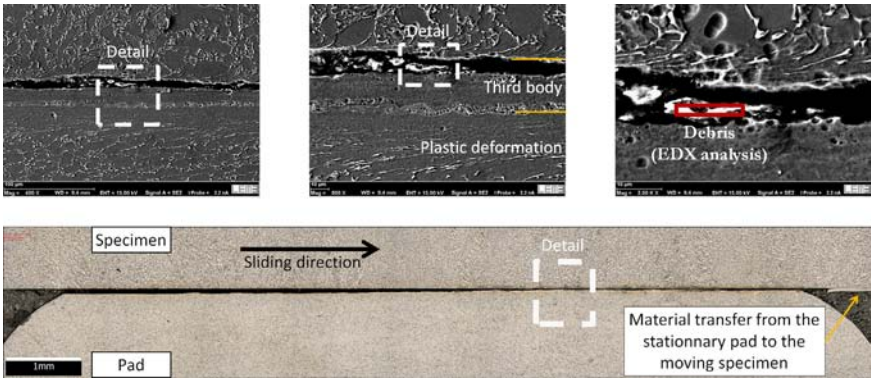

Fig. 13. SEM and optical observations of an interrupted test for an impact velocity V_{impact} of 20 m/s.

pad is focused on three spots: the front, middle and rear zones (see Fig. 5). Concerning the front zone, profile measurements revealed a significant material removal and thus, a reduction in thickness: 40 µm for the tests at 40 m/s and 20 µm at 64 m/s. In turn, the TAZ thickness is equal to 25 µm for a test at 40 m/s and 45 µm at 64 m/s. As regards the rear zone, no wear is noticeable and the TAZ thickness is 65 µm at 40 m/s and 45 µm at 64 m/s. For each sliding velocity, these measurements reveal that the sum of the wear and the TAZ thicknesses is quite constant at the three spots considered.

Volumetric measurements performed on postmortem samples are used to measure the mean wear losses. Wear rates corresponding to the ratio of wear to the interaction duration are equal to 90 mm^3/s (0.1 mm^3/1.1 ms) at 64 m/s and 180 mm^3/s (0.4 mm^3/2.2 ms) at 40 m/s. Furthermore, for a sliding length of 60 mm, the wear rate sensitively decreases with the increase of velocity and depends accordingly on interaction duration. Hale et al. [19] propose an interesting approach of mechanical wear rate calculation by numerical simulations. Although sliding conditions (steel-Vascomax 300 tribopair, normal pressure lower than 5 MPa) are hardly comparable to the present study, they also highlighted the sensitivity of wear rate to sliding velocity.

4.2.3. *Analysis of an interrupted friction test*

To better understand the evolution of the contact surface and the material transferred layer, a friction test is performed at a low initial sliding velocity of 20 m/s for 110 MPa normal pressure so that the lack of kinetic energy leads to an interrupted test. It is noted in this case that both samples are glued by a kind of friction stir welding process. Fig. 13 shows the optical and SEM observations and confirms the profile measurements in postmortem analysis: the wear occurred mainly at the front of the stationary pad. In regions where surface is still in contact, SEM examination reveals the presence of debris and voids which can be assimilated to the third body [20]. In addition, EDX analysis confirms that the debris are real particles of Ti6Al4V. Consequently, debris and compacted wear from the fixed pad are being transferred to the moving specimen during friction.

4.3. *Wear mechanism*

Fig. 14 illustrates the adhesive wear process as it occurs in the study. The wear mechanism is explained in four steps as follows:

- Intense plastic deformation takes place instantaneously all along the sliding interface. The plastic shear strain $\epsilon_{xz} = \tan(\alpha)/2$ is estimated by measuring the shear angle α on SEM images. It corresponds to the displacement of the β grains initially oriented perpendicularly to the worn surface. In our case, the maximum calculated shear strain ϵ_{xz} is up to 16.
- The interface temperature rises over 980 °C and a clear TAZ appears due to thermal diffusion in both parts in contact.
- Adhesive wear is caused by high strain level and temperatures at the contact surface. This process leads to third body generation [20]

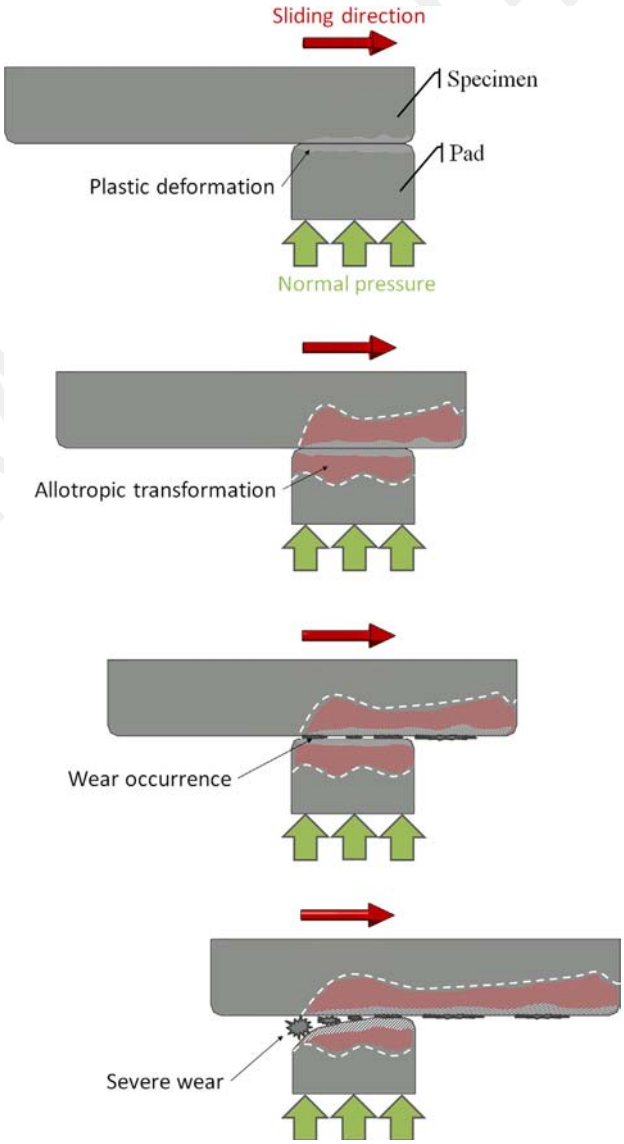

Fig. 14. Wear process for a range of sliding velocity from 40 m/s to 64 m/s for a normal pressure of 110 MPa.

consisting of debris between the sliding surfaces. As damage induced by shearing is mainly located in this third body – rather than in first bodies – wear and temperature reached at the contact interface are moderated.

- The front of the fixed pad is the only zone that keeps the original sliding conditions. The wear in this zone leads to a strong change of the contact surface area (thus a significant evolution of the stress distribution) and depends on the sliding duration. For a constant sliding length, the adhesive wear rate decreases with the increase of sliding velocity.

5. Conclusion

Friction experiments are performed in the range of 40 to 64 m/s and for an apparent normal pressure of 110 MPa. These frictional conditions are quasi instantaneously applied by the impact of a projectile against a fixed sample. The slight sensitivity of the coefficient of friction relative to the sliding velocity is estimated by means of two different methods of measurement: tribometer device and video acquisition. For the range of the studied velocities, the microstructure analyses of Ti6Al4V and worn profiles indicates

- a sub-layer decomposition: phase transformation, plastically strained layers, and material transfer,
- a material transfer from the fixed pad to the moving specimen,
- a wear mechanism occurring in four steps: a plastic deformation at the contact interface (shear strain up to 16), a thermal affected zone (TAZ) where the temperature is higher than 980 °C, an adhesive wear that modifies the sliding conditions through the formation of a third body between the two original surfaces in contact,
- an adhesive wear rate depending on sliding duration, the value of which decreases with the increase of sliding velocity for a constant sliding length.

Acknowledgments

The authors would like to thank to Région Lorraine for providing them with financial support for the acquisition of the high speed camera Shimadzu HPV2.

References

[1] M. Whittaker, Titanium in the gas turbine engine, Adv. Gas Turbine Technol. (2011) 315–336.

[2] F. Bowden, D. Tabor, The area of contact between stationary and moving surfaces, Proc. R. Soc. Lond. A 169 (1939) 391–413.

[3] S.C. Lim, M.F. Ashby, J.H. Brunton, The effects of sliding conditions on the dry friction of metals, Acta Metal. 37 (3) (1989) 767–772. http://dx.doi.org/10.1016/0001-6160(89)90003-5.

[4] M. Qiu, Y.Z. Zhang, B. Shangguan, S.M. Du, Z.W. Yan, The relationships between tribological behaviour and heat-transfer capability of Ti6Al4V alloys, Wear 263 (1–6) (2007) 653–657. http://dx.doi.org/10.1016/j.wear.2006.12.041, URL ⟨http://linkinghub.elsevier.com/retrieve/pii/S0043164807003948⟩.

[5] L. Faure, B. Bolle, S. Philippon, C. Schuman, P. Chevrier, A. Tidu, Friction experiments for titanium alloy tribopairs sliding in dry conditions: sub-surface and surface analysis, Tribol. Int. 54 (2012) 17–25. http://dx.doi.org/10.1016/j.triboint.2012.04.007, URL ⟨http://linkinghub.elsevier.com/retrieve/pii/S0301679X12001247⟩.

[6] V. Prakash, A pressure-shear plate impact experiment for investigating transient friction, Exp. Mech. 35 (4) (1995) 329–336. http://dx.doi.org/10.1007/BF02317542, URL ⟨http://www.springerlink.com/index/10.1007/BF02317542⟩.

[7] K. Ogawa, Impact friction test method by applying stress wave, Exp. Mech. 37 (4) (1997) 398–402. http://dx.doi.org/10.1007/BF02317304.

[8] H. Espinosa, A. Patanella, M. Fischer, A novel dynamic friction experiment using a modified kolsky bar apparatus, Exp. Mech. 40 (2) (2000) 138–153. http://dx.doi.org/10.1007/BF02325039.

[9] A. Bragov, A. Konstantinov, A. Lomunov, Y. Shmotin, L. Kruszka, Experimental definition of dynamic friction, DYMAT 2009—9th International Conferences on the Mechanical and Physical Behaviour of Materials under Dynamic Loading 1 (2009) 619–624. http://dx.doi.org/10.1051/dymat/2009088, URL ⟨http://www.dymat-proceedings.org/10.1051/dymat/2009088⟩.

[10] S. Rajagopalan, V. Prakash, A modified torsional kolsky bar for investigating dynamic friction, Exp. Mech. 39 (4) (1999) 295–303. http://dx.doi.org/10.1007/BF02329808, URL ⟨http://www.springerlink.com/index/10.1007/BF02329808⟩.

[11] S. Philippon, Etude expérimentale du frottement sec à grandes vitesses de glissement (Ph.D. thesis), Université de Metz, 2004.

[12] S. Philippon, G. Sutter, A. Molinari, An experimental study of friction at high sliding velocities, Wear 257 (7–8) (2004) 777–784. http://dx.doi.org/10.1016/j.wear.2004.03.017, URL ⟨http://linkinghub.elsevier.com/retrieve/pii/S0043164804000742⟩.

[13] S. Philippon, G.Z. Voyiadjis, L. Faure, A. Lodygowski, A. Rusinek, P. Chevrier, E. Dossou, A device enhancement for the dry sliding friction coefficient measurement between steel 1080 and vascomax with respect to surface roughness changes, Exp. Mech. 51 (3) (2010) 337–358. http://dx.doi.org/10.1007/s11340-010-9368-9, URL ⟨http://www.springerlink.com/index/10.1007/s11340-010-9368-9⟩.

[14] A. Lodygowski, L. Faure, G.Z. Voyiadjis, S. Philippon, Dry sliding friction experiments at elevated velocities, Strain 47 (2011) 436–453. http://dx.doi.org/10.1111/j.1475-1305.2010.00785.x, URL ⟨http://doi.wiley.com/10.1111/j.1475-1305.2010.00785.x⟩.

[15] M. Cuny, S. Philippon, P. Chevrier, F. Garcin, Experimental measurement of dynamic forces generated during short-duration contacts: application to blade-casing interactions in aircraft engines, Exp. Mech. 54 (2014) 101–114, http://dx.doi.org/10.1007/s11340-013-9780-z.

[16] R. Komanduri, Z. Hou, A review of experimental techniques for the measurement of heat and temperatures generated in some manufacturing processes and tribology, Tribol. Int. 34 (2001) 653–682.

[17] J. Puerta Velasquez, L. Lavisse, J. Kneip, H. Andrzejewski, P. Chevrier, B. Bolle, A. Tidu, S. Matteï, Thermal effects of continuous laser treatment on Ti-6 Al(wt%)-4 V(wt%) titanium alloy, Mater. Sci. Forum 595–598 (2008) 1033–1038.

[18] P. Fernandes, G.W. Haertel Jr., S. Zanotto, P.A. Sinatora, Influence of mild and severe wear condition in the formation and stability of friction film in clutch system, Wear (2013) 1384–1391. http://dx.doi.org/10.1016/j.wear.2013.02.003.

[19] C. Hale, A. Palazotto, W. Baker, Engineering approach for the evaluation of mechanical wear considering the experimental Holloman high speed test track, J. Eng. Mech. 138 (9) (2012) 1127–1140.

[20] M. Godet, Third-bodies in tribology, Wear 136 (1) (1990) 29–45. http://dx.doi.org/10.1016/0043-1648(90)90070-Q, URL ⟨http://www.sciencedirect.com/science/article/pii/004316489090070Q⟩.